Solid State Ionics 48 (1991) 155–171
North-Holland

SOLID
STATE
IONICS

Electrode polarization at the $Au,O_2(g)$/yttria stabilized zirconia interface. Part II: electrochemical measurements and analysis

B.A. van Hassel, B.A. Boukamp and A.J. Burggraaf

Laboratory for Inorganic Chemistry, Materials Science and Catalysis, Department of Chemical Technology, University of Twente, P.O. Box 217, 7500 AE Enschede, The Netherlands

Received 3 January 1991; accepted for publication 6 August 1991

The impedance of the $Au,O_2(g)$/yttria stabilized zirconia interface has been measured as function of the overpotential, temperature and oxygen partial pressure. At large cathodic overpotentials ($\eta < -0.1$ V) and large anodic overpotentials ($\eta > +0.1$ V) inductive effects are observed in the impedance diagram at low frequencies. Those inductive effects result from a charge transfer mechanism where a stepwise transfer of electrons towards adsorbed oxygen species occurs. A model analysis shows that the inductive effects at cathodic overpotentials appear when the fraction of coverage of one of the intermediates increases with more negative cathodic overpotentials. The steady state current–voltage characteristics can be analyzed with a Butler–Volmer type of equation. The apparent cathodic charge transfer coefficient is close to $\alpha_c = 0.5$ and the apparent anodic charge transfer coefficient varies between $1.7 < \alpha_a < 2.8$. The logarithm of the equilibrium exchange current density (I_0) shows a positive dependence on the logarithm of the oxygen partial pressure with a slope of $m = (0.60 \pm 0.02)$. Both the apparent cathodic charge transfer coefficient and the oxygen partial pressure dependence of I_0 are in accordance with a reaction model where a competition exists between charge transfer and mass transport of molecular adsorbed oxygen species along the electrode/solid electrolyte interface. The apparent anodic charge transfer coefficients deviate from the model prediction.

1. Introduction

In Part I [1,2] three reaction models were distinguished which can describe the oxygen exchange reaction at the noble metal/solid electrolyte interface. The first model assumes that the charge transfer reaction is rate controlling. The second model considers a competition between charge transfer and mass transport along the noble metal/solid electrolyte interface. The third model assumes that the mass transport of oxygen is rate controlling.

In this study steady state polarisation measurements have been performed on the $Au,O_2(g)$/yttria stabilized zirconia interface as a function of the oxygen partial pressure and temperature. The current-overpotential curve shows Tafel behaviour. Impedance measurements have been performed as a function of the polarisation. During cathodic and anodic polarisation inductive loops are observed at low frequencies in the impedance diagram. The experimental results are discussed in view of the reaction models of Part I [1,2].

These measurements have been performed to determine the rate determining steps in the oxygen exchange mechanism at the $Au,O_2(g)$/YSZ interface. These results will be used as comparison in a subsequent study on the influence of Fe implantation on the rate of the oxygen exchange at the $Au,O_2(g)$/yttria stabilized zirconia interface [3,2]. This effect is expected to be more easily observed with an electrode which is not catalytically active in the oxygen exchange reaction. Therefore a Au electrode was selected, instead of e.g. Pt or Ag.

2. Experimental

Yttria stabilized zirconia powder (Zircar, type: ZYP $(ZrO_2)_{0.87}(YO_{1.5})_{0.13}$) was isostatically pressed (400 MPa) and heated for three hours at both 1300 and 1400 °C. Rods were obtained with a density of 5.89 g.cm^{-3} (= 99% of theoretical density). From these rods discs were cut (diameter : 10 mm, thickness : 1 mm). The discs were mechanically polished, first with SiC (29,9,7 and 5 μm) and finally with diamond paste (7 and 3 μm). After polishing, the pellets were ultrasonically cleaned in isopropanol and finally annealed at 900 °C for 5 hours.

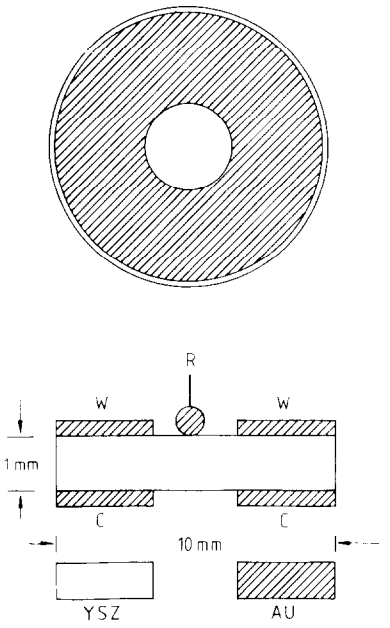

Fig.1 Geometry of the three electrode electrochemical cell. The working (W) and counter (C) electrode have an annular symmetry. The reference electrode (R) is placed in the center of the working electrode.

Annular working and counter electrodes were made by sputtering a 500 nm thick Au layer on the surface. The edge and centre of the pellet were protected against Au deposition by an aluminium mask. The pellet was sandwiched between two annular Au foils to which Au wires were attached. In the centre of the annular working electrode, where no Au was deposited, a point shaped Au electrode was pressed on the pellet and this electrode served as a reference electrode. This cell geometry is shown in fig. 1.

The cell was heated in a tubular Hereaus furnace controlled by an Eurotherm Model 810 temperature controller in the temperature range of 500-800 °C. The N_2/O_2 gas mixtures of desired ratio were obtained by a gas mixing system (Inacom instruments). Gas flow rates were kept at around 80 ml/min (STP). All electrochemical measurements were made at atmospheric pressure. The Au electrode was conditioned by heating for 12 hours at 820 °C and for two weeks at 769 °C in an oxygen atmosphere.

The steady state polarization of the Au electrode was studied in the three-electrode cell, discussed above, with a Bank pos 73 potentiostat. The potential between the reference electrode and working electrode was controlled and the steady state current between the counter and working electrode was measured. The potential was varied in a stepwise fashion and the current was determined after waiting for equilibration. After the data were collected, the applied voltage was corrected for the uncompensated resistance between the working and reference electrode to yield the overpotential. The uncompensated resistance was determined by impedance spectroscopy. The cell current density was obtained by dividing the current by the geometric area of the working electrode (0.659 cm^2).

Impedance measurements were performed in the three-electrode cell over the frequency range of 10 mHz - 100 kHz, using a Solartron 1174 frequency response analyzer. An excitation voltage of 0.010 V (rms) was added to the steady state polarization. For determination of the DC (differential) electrode resistance, the potential between the electrodes was varied ± 0.005 V around the steady state polarization used in the impedance measurements and the steady state current was measured. The resistance was determined from the slope of the steady-state current versus potential plot.

Scanning electron microscopy (SEM) micrographs were obtained from the solid electrolyte disk after about 40 days of varied history (fig. 2). After removing the strong adherent Au foil, the YSZ surface was found to be covered for 25 % with Au islands of about 1.3 μm in diameter.

Surface contaminations of both the Au electrode and the solid electrolyte were determined by SIMS and AES [4]. The SIMS apparatus (IMMA of Applied Research Laboratories) was equipped with a duoplasmatron ion source delivering a 20 keV $^{18}N^+$ ion beam with a beam diameter of 1.5 μm. The secondary ions were mass selected in a magnetic sector analyzer. The SIMS analysis was performed at room temperature.

3. Results

3.1. *Surface analysis*

The surfaces of both the Au electrode and yttria stabilized zirconia solid electrolyte were analyzed for surface impurities by SIMS. Surface impurities are thought to influence the adsorption of oxygen on both the solid electrolyte and Au electrode. The major impurities detected in the positive ion spectrum of the surface of the stabilized zirconia solid electrolyte are Na, Mg, Al, Si, K and Ca. The amount of those surface impurities could not be quantified as the sensitivity factors for each element with respect to the matrix were unknown. It should be noted that the SIMS technique is extremely sensitive to cations like Na and K. In the negative ion spectrum a small amount of Cl and carbon was detected.

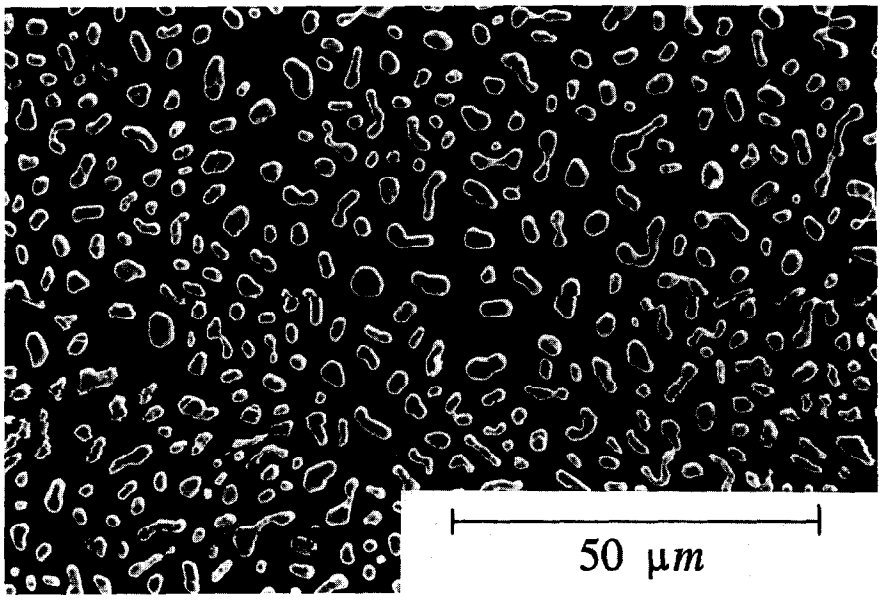

Fig.2 SEM micrograph of a porous Au electrode after about 40 days of varied history.

After sputtering a 500 nm thick film of Au on the yttria stabilized zirconia surface, the Au electrode was annealed at 800 °C for 17 hours in air. The surface impurities detected on the solid electrolyte surface were also found on the Au electrode. The Au electrode contained also a small amount of Rh. The negative ion spectrum showed the presence of some (adsorbed) oxygen on the Au electrode.

3.2. *Steady state polarization*

Some hysteresis was observed in most of the current-overpotential curves obtained from the Au,O_2(g)/stabilized zirconia interface. The current during the forward sweep, defined for negatively swept potentials, was slightly smaller than the current on the reverse sweep. The latter was more reproducible and for that reason the current-overpotential curve obtained after increasing the potential from -0.7 V to +0.2 V is shown in fig. 3.

The current overpotential curve of fig. 3 can be analyzed with the Butler-Volmer equation, as discussed in Part I [1]. In order to obtain values of the apparent charge transfer coefficients and the equilibrium exchange current density, the current-overpotential curves were transformed into Tafel-plots. Figure 4 shows a typical result. From the slope of the cathodic and anodic branch of the Tafel plot, values can be calculated for the apparent cathodic (α_c) and anodic (α_a) charge transfer coefficients respectively. Extrapolation of these linear segments to a zero overpotential results in the logarithm of the equilibrium exchange current density (I_o). Both the values of the apparent charge transfer coefficients and the oxygen partial pressure dependence of the equilibrium exchange current density contain important information about the electrode mechanism.

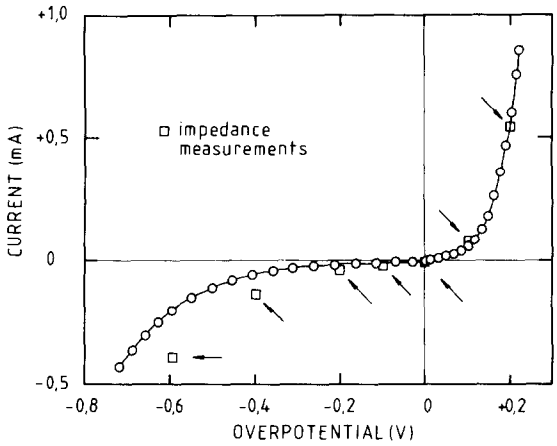

Fig.3 Current-overpotential curve of a porous Au electrode on yttria stabilized zirconia at 769°C and an oxygen partial pressure of PO_2=1 atm. The over-potentials at which the electrode impedance has been measured are indicated.

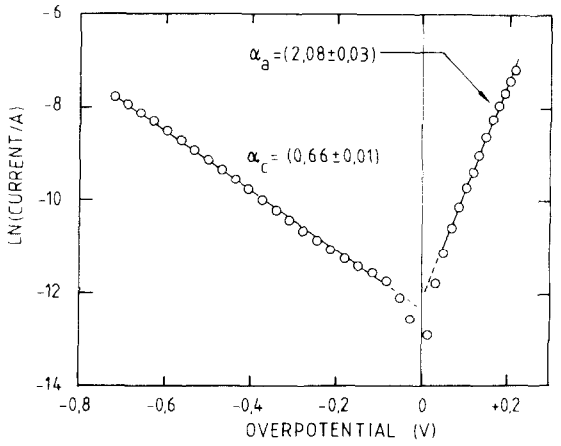

Fig.4 Tafel plot of the current-overpotential curve of fig. 3.

Results for the apparent charge transfer coefficients as a function of the temperature at an oxygen partial pressure of P_{O_2}=1 atm are shown in fig. 5. The apparent anodic charge transfer coefficient decreased from α_a=2.2 at 800 °C to α_a=1.7 at 500 °C, whereas the apparent cathodic charge transfer coefficient was always close to α_c=0.5 in the temperature range of 500 to 800 °C. The equilibrium exchange current density as a function of the temperature at an oxygen partial pressure of P_{O_2}=1 atm is shown in fig. 6. The activation energy of the equilibrium exchange current density is (112±2) kJ mol^{-1}.

Tafel plots as a function of the oxygen partial pressure at a temperature of 769 °C are shown in fig. 7. In order

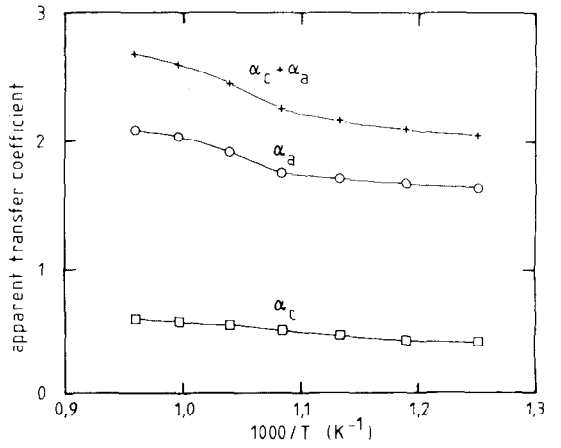

Fig.5 Apparent charge transfer coefficients as function of the reciprocal absolute temperature at PO_2=1 atm.

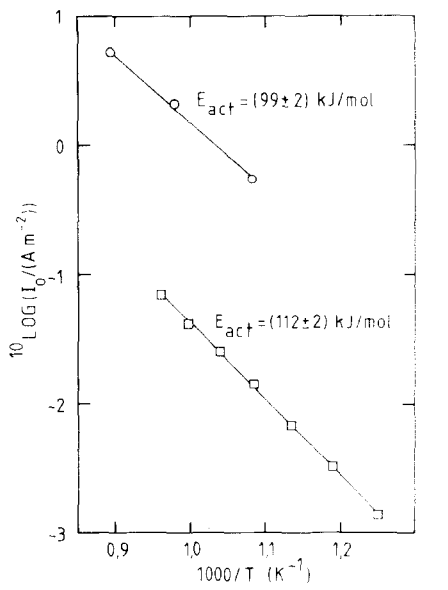

Fig.6 Arrhenius-plot of the equilibrium exchange current density, (□) our study, (○) Nguyen et al. [25].

to obtain this fig. each Tafel plot was displaced by the Nernst potential taking P_{O_2}=1 atm as the reference gas. This means that the overpotential can be obtained by substracting from the electrode potential, the corresponding Nernst potential. Tafel behaviour is observed over the entire oxygen partial pressure range studied (10^{-5} to 1 atm). Results for the apparent charge

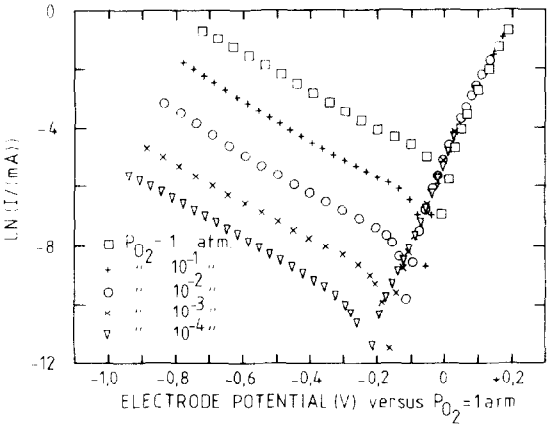

Fig.7 Tafel-plots of the Au,O_2(g)/yttria stabilized zirconia interface measured at 769°C and at oxygen partial pressures in the range of 10^{-4} to 1 atm. The electrode potential is defined versus the equilibrium potential at 769°C and PO_2=1 atm.

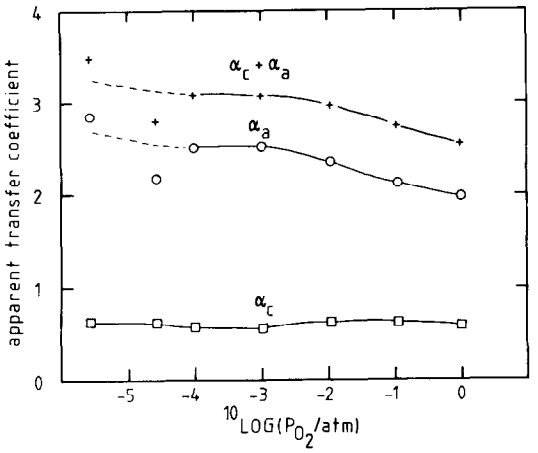

Fig.8 Apparent charge transfer coefficients as function of the oxygen partial pressure at 769°C (obtained from fig. 7).

transfer coefficients as a function of the oxygen partial pressure are given in fig. 8. The apparent anodic charge transfer coefficient varies from $\alpha_a=2$ at $P_{O_2}=1$ atm to $\alpha_a=2.6$ at $P_{O_2}=10^{-5}$ atm. The apparent cathodic charge transfer coefficient is independent of the oxygen partial pressure and has a value close to $\alpha_c=0.5$. Results for the P_{O_2} dependence of the exchange current density, as studied at 769 °C, are given in fig. 9. Log I_o shows a positive dependence on log P_{O_2}, with a slope of $m=(0.60\pm0.02)$. The deviation of the measured I_o values

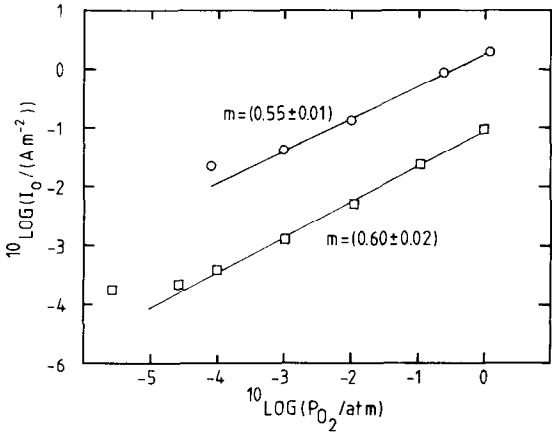

Fig.9 Equilibrium exchange current density (□) as function of the oxygen partial pressure at 769°C obtained from fig. 7. For comparison the exchange current density presented by Nguyen et al. [25] is shown (○).

from this slope at low oxygen partial pressures results probably from impurities like H_2O or CO_2 [5].

The results concerning the Tafel slopes, activation energy of I_o and P_{O_2} dependence of I_o could be well reproduced from sample to sample. The absolute value of I_o could only be reproduced within a factor of 2.

3.3. *Impedance spectroscopy*

3.3.1. *Polarized interface*

Frequency dependent impedance measurements have been performed as a function of the overpotential between the working and reference electrode at a temperature of 769 °C and $P_{O_2}=1$ atm. The overpotential values where the impedance measurements were performed are indicated in the current-overpotential curve of fig. 3. The impedance measurements were analyzed with the computer program "Equivalent Circuit" [6,7]. The equivalent circuit that was found to reproduce most closely the impedance diagrams is shown in fig. 10. A list of equivalent circuit elements, the corresponding symbols and dispersion relations can be found in [6,7]. The values of the equivalent circuit elements, are tabulated in table 1.

At cathodic overpotentials smaller than $\eta=-0.1$ V, an inductive loop appears at low frequencies in the impedance diagram as is shown in the fig.s 11a and 11b, for the case of $\eta=-0.596$ V and $\eta=-0.4$ V, respectively. At a cathodic overpotential of $\eta=-0.1$ V only one depressed semicircle is observed (fig. 11c) belonging to the parallel combination of R_{ct} and C_{dl} in the equivalent circuit of fig. 10. The impedance diagram at zero overpotential (fig. 11d) is discussed in section 3.2.2. At an anodic overpotential of $\eta=+0.1$ V, a capacitive loop develops at low frequencies in the impedance diagram, as shown in fig. 11e. A further increase in anodic overpotential results again in the development of an inductive loop at low frequencies in the impedance diagram, as is shown in fig.

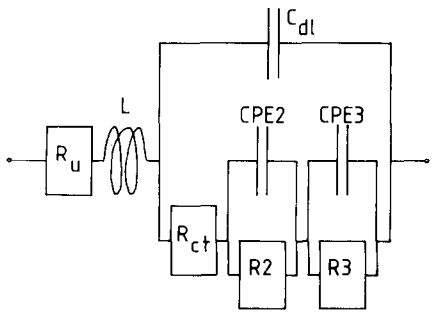

Fig.10 Equivalent circuit used in the NLLS-fit analysis of the impedance diagrams of fig. 11.

Table 1 Values of the equivalent circuit element parameters obtained from the NLLS-fit analysis of the electrode impedances presented in fig. 10. Resistances are expressed in ohms, the Y_0 parameters of the constant phase elements sec^n ohm^{-1}, where n is their exponent value.

Equivalent circuit element	Overpotential (V)					
	-0.596	-0.400	-0.100	0	0.100	0.199
R_u	17	19	21	22	22	22
C_{dl}	$2.7x10^{-6}$	$3.2x10^{-6}$	$8.1x10^{-6}$	$8.0x10^{-6}$	$8.3x10^{-6}$	$7.3x10^{-6}$
n_{dl}	0.87	0.86	0.80	0.81	0.82	0.81
R_{ct}	421	1204	8562	2770	468	125
R2	40	129	464	554	58	46
CPE2	$1.1x10^{-2}$	$1.4x10^{-3}$	$0.3x10^{-3}$	$2.7x10^{-3}$	$0.7x10^{-3}$	$10.3x10^{-3}$
n2	-0.53	-0.79	-0.75	0.48	0.79	1.00
R3	216	201	253			15
CPE3	$44.4x10^{-3}$	$29.4x10^{-3}$	$0.9x10^{-3}$			$1.3x10^{-3}$
n3	-0.57	-0.69	1.00			-0.39

11f for the case of $\eta = +0.199$ V. The low frequency features in the impedance diagram are assumed to result from the concentration impedance of adsorbed oxygen species as represented by the equivalent circuit parameters R2, CPE2, R3 and CPE3 in fig. 10. The dispersion relation for a constant phase element (CPE) is expressed by (in admittance form):

$$Y(\omega) = Y_o(j\omega)^n \qquad (1)$$

As can be seen from fig. 11, the time constants of the different elements in the equivalent circuit overlap severely. The differences in time constants changed from sample to sample, but in all cases inductive loops appeared at large cathodic and anodic overpotentials.

The first resistance, R_u, in the equivalent circuit of fig. 10 is interpreted as the uncompensated resistance between the working and reference electrode. As is shown in fig. 12 this resistance is independent of the overpotential between the working and reference electrode, in the potential range studied.

The first constant phase element, C_{dl}, is interpreted as a kind of double layer capacitance, which is in parallel with the Faradaic impedance of the Au electrode. The Y_o value of this constant phase element is a function of the overpotential, as shown in fig. 13. A maximum appears in the double layer capacitance versus overpotential plot under equilibrium conditions, when no overpotential is applied. The exponent value, n, of this constant phase element varies around 0.8, indicating that this constant phase element resembles a pure capacitance, in which case $n = 1$.

From the DC point in the impedance diagram the electrode resistance, R_{el}, can be calculated by substracting the uncompensated resistance, R_u. The electrode resistance is exponentially dependent on the applied overpotential, as shown in fig. 12. This can be expected from the Butler-Volmer equation. Almost the same apparent cathodic charge transfer coefficient ($\alpha_c = 0.53 \pm 0.03$) results from fig. 12 as calculated from the cathodic Tafel slope of the current-overpotential curve ($\alpha_c = 0.66 \pm 0.01$), shown in fig. 7. The apparent anodic charge transfer coefficient ($\alpha_a = 1.4 \pm 0.1$) deviates more seriously from the one of the Tafel-plot ($\alpha_a = 2.08 \pm 0.03$), possibly due to the longer stabilisation time in the impedance measurements. Figure 12 shows also that the main contribution to the electrode resistance is given by the charge transfer resistance, R_{ct}.

The parallel combination of R2, CPE2, R3 and CPE3 in fig. 10 will be called the concentration impedance of the adsorbed oxygen species, in order to facilitate the discussion of the results. The concentration impedance of the adsorbed oxygen species shows a complicated behaviour as a function of the overpotential. It behaves as an inductive loop at large cathodic overpotentials, but as a capacitive loop at relative small anodic overpotentials. At higher anodic overpotentials, both a capacitive and inductive loop are observed.

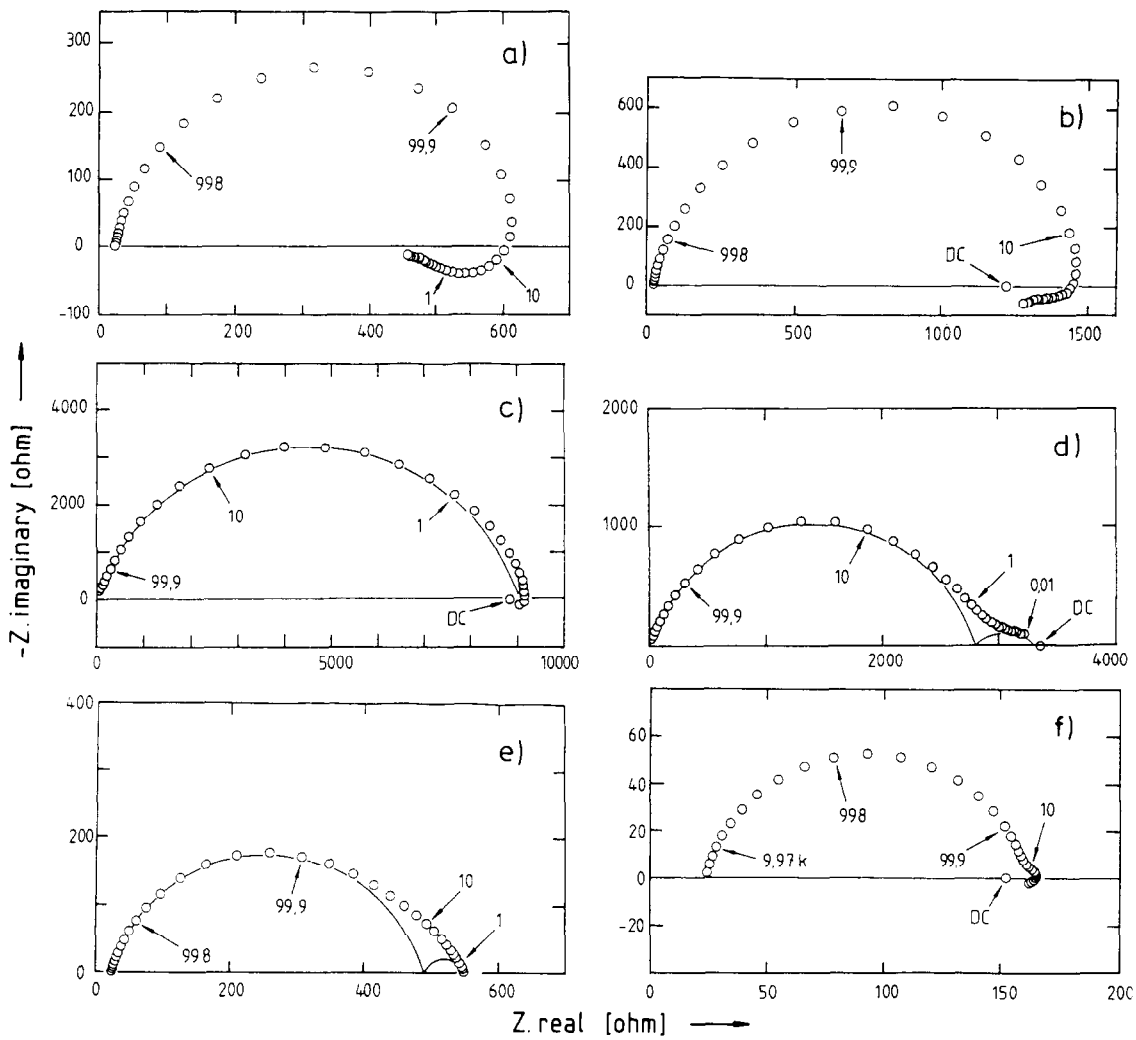

Fig.11 Impedance diagrams (769°C, PO_2=1 atm) for a porous Au electrode on YSZ as function of the overpotential: a) η=-0.596 V, b) η=-0.400 V, c) η=-0.100 V, d) η=0 V, e) η=0.100 V, f) η=0.199 V. Frequencies indicated in Hz.

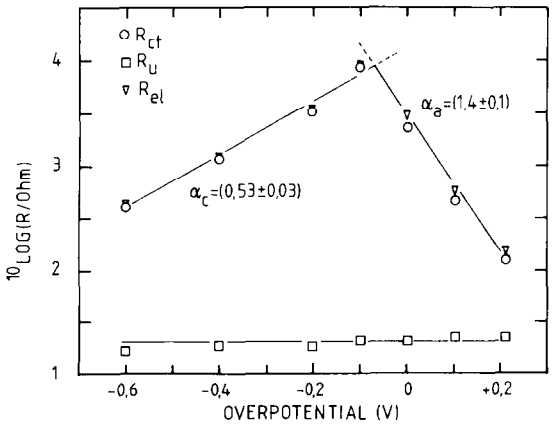

Fig.12 Uncompensated resistance (R_u), charge transfer resistance (R_{ct}), and electrode resistance (R_{el}) as function of the overpotential at PO_2=1 atm and 769°C.

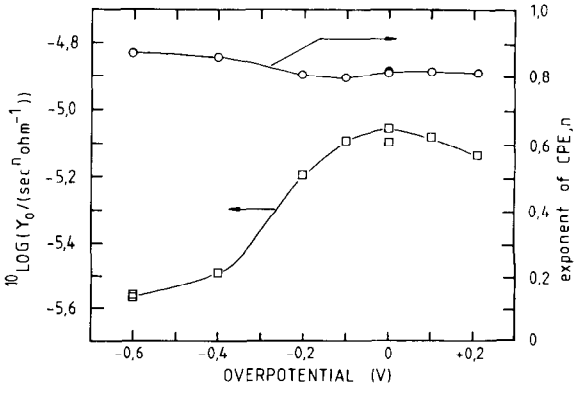

Fig.13 Double layer capacitance (C_{dl}) and the exponent n of this constant phase element as function of the overpotential at 769°C and PO_2=1 atm.

3.3.2. *Unpolarized interface*

Frequency dependent impedance measurements have been performed at zero overpotential as a function of the temperature and oxygen partial pressure. A typical impedance diagram, obtained under equilibrium conditions (η=0 V) at 769 °C and Po_2=1 atm is shown in fig. 11d. At zero overpotential a depressed semicircle is observed in the impedance plot. Upon close examination, an additional depressed capacitive loop proves to be present at the low frequency site of the impedance diagram. The appropriate equivalent circuit is shown in fig. 10. In comparison to the polarized interface, however, only one parallel combination of a resistance, R2 and constant phase element CPE2 is present. The second parallel combination of a resistance, R3, and constant phase element, CPE3, is not observed at zero overpotential.

The first resistance, R_u, in the equivalent circuit is interpreted as the uncompensated resistance between the working and reference electrode. In fig. 14 an Arrhenius-plot is shown of this uncompensated resistance. The activation energy of R_u is (104±2) kJ mol^{-1}. In fig. 15 it is shown that the uncompensated resistance, R_u, is independent of the oxygen partial pressure.

The first constant phase element, C_{dl}, is once again interpreted as an apparent double layer capacitance, which is in parallel to the Faradaic impedance of the Au electrode. Some increase in the double layer capacitance is observed in fig. 16 with an increase in temperature. In fig. 17, a decrease of the double layer capacitance is

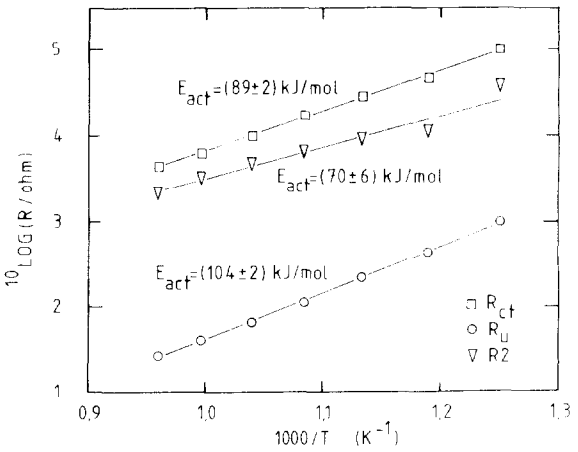

Fig.14 Arrhenius-plot (PO_2=1 atm) of the resistances R_u, R_{ct} and R2 of the equivalent circuit of fig. 10.

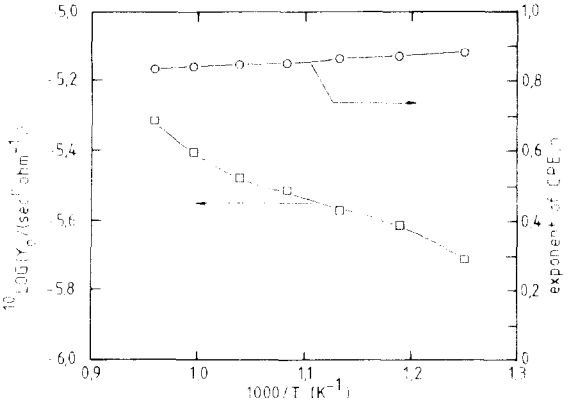

Fig.16 Double layer capacitance (C_{dl}) and the exponent n of this constant phase element as function of the reciprocal absolute temperature at PO_2=1 atm.

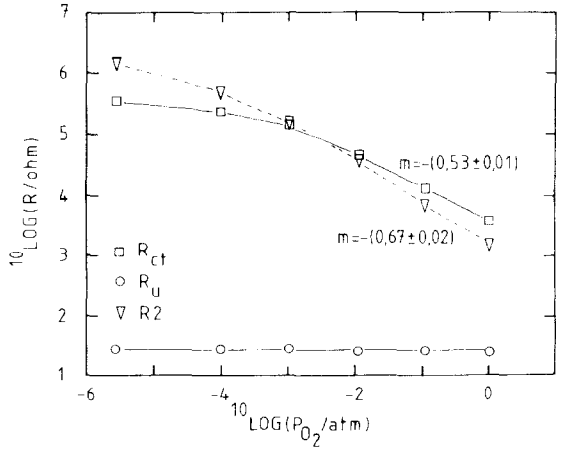

Fig.15 Oxygen partial pressure dependence of the resistances R_u, R_{ct} and R2 at 769°C.

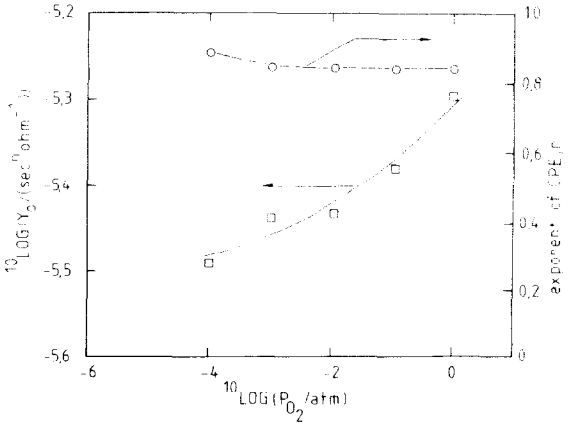

Fig.17 Double layer capacitance (C_{dl}) and the exponent n of this constant phase element as function of the oxygen partial pressure at 769°C.

observed with a decrease of the oxygen partial pressure. The exponent value n of this constant phase element varies between 0.8 and 0.9 as also shown in fig. 16 and 17. This indicates that this constant phase element closely resembles a pure capacitance, for which n=1.

The Faradaic impedance of the electrode consists of a charge transfer resistance, R_{ct}, in series with a parallel combination of a constant phase element, CPE2 and a resistance, R2. From the Arrhenius-plot of R_{ct} in fig. 14 an activation energy of R_{ct} is obtained of (89±2) kJ mol^{-1}. The oxygen partial pressure dependence of the R_{ct} is shown in fig. 15. The charge transfer resistance depends on the oxygen partial pressure as: $R_{ct} \propto Po_2^{-(0.53\pm0.01)}$ in the oxygen partial pressure range of 10^{-3} to 1 atm.

The concentration impedance of the adsorbed oxygen species, represented by the parallel combination of R2 and CPE2 in the equivalent circuit of fig. 10, was always present as a capacitive loop at zero overpotential. The activation energy of R2 is (70±6) kJ mol^{-1} as shown in fig. 14. The resistance R2 is strongly dependent on the oxygen partial pressure according to $R2 \propto Po_2^{-(0.67\pm0.02)}$ in the oxygen partial pressure range of 10^{-3} to 1 atm as is shown in fig. 15. The temperature dependence of CPE2 is shown in fig. 18 and its value is two orders of magnitude larger than the double layer capacitance, C_{dl}. The exponent value n of CPE2 varies between 0.5 and 0.6 as also shown in fig. 18 so that it resembles a Warburg impedance for semi-infinite diffusion, for which case n=0.5. At high oxygen partial pressures, the contribution of the parallel combination of R2 and CPE2 to the electrode impedance was always small in comparison to that of the parallel combination of the charge transfer resistance and the apparent double layer capacitance. The oxygen partial pressure dependence of CPE2 in the

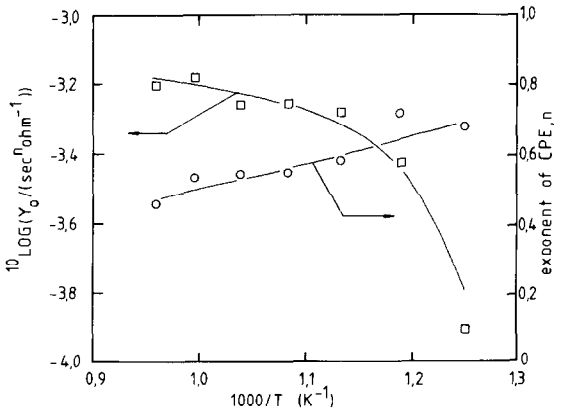

Fig.18 The Y_0 value of CPE2 and the exponent n as function of the reciprocal absolute temperature at PO_2=1 atm.

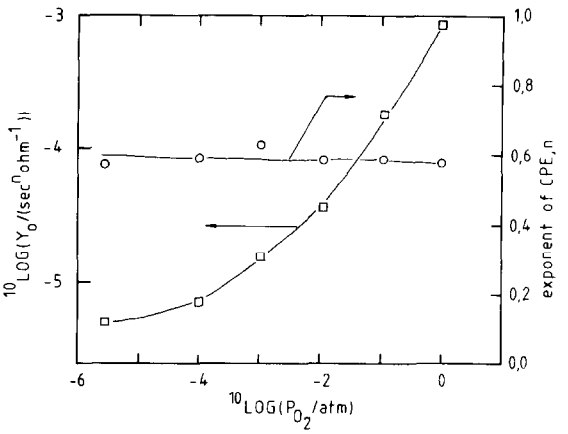

Fig.19 The Y_0 value of CPE2 and the exponent n as function of the oxygen partial pressure at 769°C.

equivalent circuit of fig. 10 is shown in fig. 19. A decrease of the value of CPE2 with two orders of magnitude is observed when the oxygen partial pressure is decreased from Po_2=1 atm to $Po_2=10^{-6}$ atm. The exponent value of this CPE2 is still between 0.5 and 0.6. At low oxygen partial pressures, the parallel combination of R2 and CPE2 mainly determines the electrode impedance.

4. Discussion

4.1. Oxygen adsorption

In all reaction models the first step in the reaction mechanism consists of the adsorption of oxygen either on the noble metal electrode or on the stabilized zirconia surface. In the past many investigations were aimed at understanding the adsorption of oxygen on gold [8-13]. All those studies show the essential role played by impurities in the interaction of oxygen with Au surfaces. If Ca or Si are present as impurities in gold, an oxide layer may form which is stable up to 800 °C [8-12]. No oxygen adsorption was found on Au free of those impurities [13].

The presence of those impurities in the porous Au films used in this study was investigated with both AES and SIMS [4]. Prior to the surface analysis the sputtered Au film was annealed at 800 °C during 17 hours in air. No Si or Ca could be detected with AES, but SIMS revealed the presence of Na,Mg,Al,Si,K and Ca as the most important impurities. Another important surface impurity proved to be Rh. The amount of the surface impurities could not be quantitatively determined, but was below the detection limit of the AES-technique. As the sputtered Au film was not free of impurities some adsorption of oxygen may be expected and it might not be

as inert in the oxygen exchange reaction as previously assumed.

More recent studies show that the catalytic activity of Au metal in the oxidation of CO and H_2 in air depends markedly on the crystallite size and the supporting oxide [14,15]. However, Au supported on ZrO_2 proved to be relatively inert in the oxidation of CO or H_2 in air in comparison to Au supported on the oxides of group VIII 3d transition metals. In view of the particle size of the Au electrode used in this study and stabilized zirconia as a "support", no high catalytic activity can be expected in the present study.

The adsorption of oxygen on stabilized zirconia has been studied less intensively than that on Au. Meas [16] concluded from his measurements that the number of adsorption sites for oxygen was approximately equal to the number of oxygen vacancies at the surface. Smith [17,18] concluded from his adsorption/desorption measurements of oxygen on pure ZrO_2 that approximately 5% of a monolayer of oxygen could be reversibly adsorbed. The kinetics of the adsorption/desorption reaction suggested that electrons from the conduction band of ZrO_2 were transferred to the molecularly adsorbed oxygen, which formed a mobile adsorption layer.

The exchange rate of oxygen on stabilized zirconia was investigated with ^{18}O isotope exchange measurements by a number of investigators [19-21]. As shown by Kurumchin [19], the isotopic exchange rate (R) was thermally activated with an activation energy of 100 kJ mol^{-1}. The logarithm of the isotopic exchange rate was linearly dependent on the logarithm of the oxygen partial pressure with a slope of m=0.25. Tannhauser [20] and Steele [21] showed that the surface exchange rate was relatively slow and influenced the diffusion profile of ^{18}O within the solid.

The adsorption of oxygen has been more intensively studied on other oxides. ESR measurements [22,23] has so far given the most detailed knowledge about adsorbed oxygen species on oxides. From those measurements it was concluded that the following oxygen species were sufficiently characterized on the surface, to be used with confidence in mechanistic studies: $O_{2,ad}$, $O^-_{2,ad}$, $O^{2-}_{2,ad}$, O^-_{ad}, O_2 in low coordination and oxygen coordinated to a metal cation (M=O). Most ESR measurements are performed at low temperature and it is expected that those oxygen species may easily transform at higher temperatures where catalytic reactions take place. More evidence concerning charge transfer of electrons to adsorbed oxygen species resulted from changes in work function and surface conductivity of semiconducting oxides [24].

Thus it can be concluded that during our electrochemical measurements, oxygen may adsorb either on the slightly contaminated Au electrode or on the stabilized zirconia surface. Different adsorbed oxygen species may be present. Some influence of the adsorption site on the reactivity of the oxygen species can be expected, but to our knowledge no detailed studies about this influence have appeared in literature.

4.2. *Reaction model*

In Part I [1], three types of reaction models were distinguished which were proposed to describe the oxygen exchange at the noble metal,O_2(g)/yttria stabilized zirconia interface. The differences between the models were emphasised as far as it concerned the expressions for the steady state current-overpotential curve and the electrode impedance. The experimental results obtained in this paper are discussed in view of those reaction models.

4.2.1. *Steady state polarisation*

In the temperature range of 500-840 °C and in the Po_2 range of 10^{-6}-1 atm the current overpotential curve obeys a Butler-Volmer type of equation. The value of the apparent charge transfer coefficients for the cathodic site of the current overpotential curve is always close to $\alpha_c=0.5$. The value of the apparent charge transfer coefficient for the anodic reaction varies from $\alpha_a=1.7$ to $\alpha_a=2.8$. This results in a sum of the cathodic and anodic apparent charge transfer coefficient, which varies from 2.2 to 3.3. No limiting current was observed in the overpotential range studied ($-0.8<\eta<+0.2$ V).

From this result it can be concluded that the rate of the oxygen exchange reaction is not limited by a mass transport process as proposed by Mizusaki [25,26], who studied the electrode reaction at the Pt,O_2(g)/stabilized zirconia interface. In that model it is assumed that the equilibrium exchange current density is infinite high and limiting currents are predicted at relative low values of the applied overpotential ($\eta>0.3$ V). No limiting currents were observed in this study. So other processes apart from pure mass transport must be considered to be rate determining in the case of the oxygen exchange reaction at the Au,O_2(g)/stabilized zirconia interface.

Apparent Tafel behaviour results from either a pure charge transfer process or from a competition between the charge transfer process and mass transport along the Au,O_2(g)/stabilized zirconia interface. This was discussed in detail in Part I [1]. In both reaction models it is possible to obtain an apparent cathodic charge transfer coefficient $\alpha_c=0.5$ and apparent anodic charge transfer coefficient $\alpha_a=1.5$. The sum of both charge transfer coefficients equals a whole number which in both cases should be equal to 2. The apparent cathodic charge transfer coefficient, as experimentally determined, was found to be close to $\alpha_c=0.5$ and proved to be independent

of the temperature and oxygen partial pressure, as shown in fig. 5 and 8. The apparent anodic charge transfer coefficient varied with temperature and oxygen partial pressure from α_a=1.7-2.8, as also shown in fig. 5 and 8. This deviation from the predicted value of 1.5 is presently not understood.

One possible explanation concerns the principle of microscopic reversibility. In view of this principle the rate limiting step for forward and reverse reactions must be the same. If this principle is violated, then it is no longer necessary that the sum of the cathodic and anodic charge transfer coefficient is an integer. This line of arguments was presented by Badwal [26] in order to describe the oxygen exchange at the Pt,$(U_{0.7}Y_{0.3})O_{2+x}$,O_2(g)/yttria stabilized zirconia interface. In the electrode mechanism different reaction steps were determining the rate of the oxygen dissolution and oxygen evolution reaction.

It should be noted that Nguyen et al. [27] observed a cathodic charge transfer coefficient α_c=0.5 and an anodic charge transfer coefficient α_a=1.5 at temperatures lower than 800 °C and an oxygen partial pressure in the range 10^{-4} - 1 atm. The anodic charge transfer coefficient of α_a=1.5 could not be reproduced in this study. The main difference between our and their study concerns the electrode morphology. The Au electrode used by Nguyen et al. [27] consisted of a 5-8 μm thick Au film, which was made porous by sintering at 850 °C. The Au electrode used in our study consisted of a 500 nm thick Au film which agglomerated into Au islands of about 1.3 μm in diameter, as shown in fig. 2. Contact to the Au islands was made with a Au foil. It is assumed that due to this Au foil the three phase area between the Au electrode, solid electrolyte and gas phase was less accessible for oxygen than the porous Au electrode of Nguyen, but this assumption is difficult to verify. This may result in a high oxygen partial pressure at the electrode/solid electrolyte interface during oxygen evolution at anodic overpotentials. As discussed by Schouler and Kleitz [28] and Yanagida [5], at such high oxygen partial pressure holes may be injected in the solid electrolyte resulting in a larger effective electrode area. Such an enlargement of the electrode area during anodic polarisation will present itself in a faster increase of the current as a function of the overpotential than calculated on the basis of a constant electrode surface area.

An important distinction between a pure charge transfer process and a charge transfer process in competition with mass transport along the Au,O_2(g)/yttria stabilized zirconia interface concerns the P_{O_2} dependence of the equilibrium exchange current density. This analysis was described in Part I [1]. Often the equilibrium exchange current density can be assumed to depend on the oxygen partial pressure as:

$$I_o \propto \left(P_{O_2}\right)^m \qquad (2)$$

If the rate of the oxygen exchange reaction is determined only by a charge transfer process, and apparent charge transfer coefficients are observed of α_c=0.5 and α_a=1.5 then the equilibrium exchange current density I_o should depend on the oxygen partial pressure as given by eq. (2), with m=3/8, provided that the fraction of coverage of the adsorbed oxygen species is small ($\theta << 1$). If the charge transfer process is in competition with mass transport of molecular oxygen species then the same apparent charge transfer coefficients can be predicted but in that case the equilibrium exchange current density should depend on the oxygen partial pressure as given by eq. (2) with m=5/8, provided again that the fraction of coverage of the adsorbed oxygen species is small ($\theta << 1$). The experimentally observed equilibrium exchange current density depends on the oxygen partial pressure as given by eq. (2) with m=(0.60±0.02) which is close to m=5/8. Thus the experimentally observed P_{O_2} dependence of I_o and the cathodic charge transfer coefficient (α_c=0.5) point to the reaction model in which the charge transfer process is in competition with the mass transport of molecular oxygen along the Au,O_2(g)/yttria stabilised zirconia interface. The anodic charge transfer coefficient ($1.7 < \alpha_a < 2.8$) deviates from the model prediction (α_a=1.5). Following the assumptions in the reaction model it can also be concluded that the fraction of coverage of the molecular adsorbed oxygen is small.

A discussion of the steady state electrode polarisation at the Au,O_2(g)/yttria stabilized zirconia interface has been presented recently by Nguyen et al. [27]. In their study the I_o was temperature dependent with an activation energy of (99±2) kJ mol^{-1} which is lower than the activation energy determined in our study, i.e. (112±2) kJ mol^{-1}. The oxygen partial pressure dependence for I_o determined by Nguyen et al. [27] was given by eq. (2) with m=(0.55±0.01) which is slightly lower than that observed in our study, m=(0.60±0.02). However, the absolute value of the equilibrium exchange current density at P_{O_2}=1 atm found by Nguyen et al. [27] is a factor 20 higher than the equilibrium exchange current density observed in this study. This large difference is shown in the Arrhenius-plot of fig. 6. Such a large difference in the value of the equilibrium exchange current density was previously found in studies of the Pt,O_2/stabilized zirconia interface and results partly from different electrode morphologies [25,26,29]. Another important reason concerns the differences in surface impurities of both the Au electrode and solid electrolyte surface.

The charge transfer mechanism for the reaction model with pure charge transfer is different from the one where a competition occurs between charge transfer and mass

transport. The relation between model parameters and charge transfer coefficients was discussed in Part I [1]. From this analysis it can be concluded that when the charge transfer is rate determining and the mass transport is infinitely fast, values of $\alpha_c=0.5$ and $\alpha_a=1.5$ can be obtained if one electron is transferred in the rate determining step and two electrons are transferred after the rate determining step. In this analysis it has been assumed that the symmetry coefficient $\beta=0.5$. A typical electrode mechanism satisfing those constraints was discussed in Part I and is shown in the eqs (3a-c):

$$O_{2,(gas)} + 2\,ad \underset{k_{des}}{\overset{k_{ad}}{\rightleftarrows}} 2\,O_{ad} \qquad (3a)$$

$$2\,x\ \left(O_{ad} + e^- \underset{k_{O1}}{\overset{k_{r1}}{\rightleftarrows}} O_{ad}^-\right) \qquad (3b)$$

$$2\,x\ \left(O_{ad}^- + e^- + V_O^{\bullet\bullet} \underset{k_{O2}}{\overset{k_{r2}}{\rightleftarrows}} O_O^x + ad\right) \qquad (3c)$$

where 'ad' is an adsorption site. In this reaction mechanism step (3b) should be rate determining in order to obtain the mentioned charge transfer coefficients.

If a competition exists between a charge transfer process and mass transport along the two dimensional interphase between the noble metal electrode and the solid electrolyte then the charge transfer process should be different in order to explain the observed apparent charge transfer coefficients. In that case the charge transfer process should result in charge transfer coefficients of: $\alpha_c=\alpha_a=1$. This means that no electrons are transferred in the rate determining step and two electrons are transferred before and two after the rate determining step, assuming once again that the symmetry coefficient equals $\beta=0.5$. A typical electrode mechanism satisfying those constraints is shown in the eqs (4a-d):

$$O_{2,(g)} + ad + e^- \rightleftarrows O_{2,ad}^- \qquad (4a)$$

$$O_{2,ad}^- + ad + e^- \rightleftarrows 2\,O_{ad}^- \qquad (4b)$$

$$2\,x\ \left(O_{ad}^- + V_O^{\bullet\bullet} \rightleftarrows O_O^{\bullet} + ad\right) \qquad (4c)$$

$$2\,x\ \left(O_O^{\bullet} + e^- \rightleftarrows O_O^x\right) \qquad (4d)$$

In this reaction mechanism reaction step (4c) should be rate determining in order to obtain the desired values of charge transfer coefficients ($\alpha_c=\alpha_a=1$). Like in the electrode mechanism shown in the eqs (3a-c), a stepwise transfer of electrons takes place towards adsorbed intermediates. The implications of a reaction mechanism where a stepwise transfer of electrons takes place to adsorbed intermediates for the electrode impedance is discussed below. It is shown that inductive effects may result from such a charge transfer mechanism.

4.2.2. Electrode impedance

Original results for the oxygen exchange reaction have been obtained by impedance spectroscopy. As a first step the impedance measurements were analyzed with the computer program 'Equivalent Circuit' [6,7]. During this analysis an equivalent circuit is constructed which can describe mathematically the observed electrode impedance. The residual error after the fit procedure was less than 2 %. As a second step the consequences of the equivalent circuit for the reaction model must be considered.

The resistance R_u in the equivalent circuit of fig. 10 is attributed to the uncompensated resistance between the working and reference electrode. This resistance is thermally activated with an activation energy of $E_{act}=(104\pm2)$ kJ mol^{-1}, which is not significantly different from the activation energy of ionic conductivity ($E_{act}=(106\pm1)$ kJ mol^{-1}). The latter was determined by a four point probe measurement technique on a bar shaped sample of the solid electrolyte (ZY13). The uncompensated resistance is independent of the oxygen partial pressure, as shown in fig. 13. This can be expected as R_u is determined by the ionic conductivity of the YSZ solid electrolyte which is also independent of the oxygen partial pressure.

The uncompensated resistance was also potential independent in the range of -0.8 to +0.3 V, as shown in fig. 12, so that it is allowed to use the value of the uncompensated resistance determined under equilibrium conditions, when the net current is zero, for non equilibrium situations. This has been done when correcting the current voltage curve for the ohmic polarisation loss between the working and reference electrode.

The inductive element, L, in the equivalent circuit of fig. 10 manifests itself at high frequencies in the impedance diagram. It results from the measuring device (potentiostat) itself and the electrical connections to the cell. This inductance determines the maximum frequency at which data of the electrode impedance can be obtained accurately (generally up to 10 kHz).

The high frequency capacitive loop in the impedance diagram is interpreted as an apparent double layer capacitance, C_{dl} in parallel to the Faradaic impedance of the electrode. The value of the double layer capacitance proved to be frequency dependent. Mathematically this

was taken into account by using a constant phase element rather than a pure capacitance in the equivalent circuit of fig. 10. The exponent of this constant phase element has a mean value of: $n=0.85\pm.03$, which is close to $n=1$, as expected for a pure capacitance. The frequency dependence of this apparent double layer capacitance points to a distribution of relaxation times, to surface roughness at the electrode (fractal behaviour) or in more general terms to an inhomogeneous current distribution over the electrode.

The apparent double layer capacitance C_{dl} depends on the temperature and oxygen partial pressure, as shown in the fig.s 16 and 17. This is thought to originate from changes in the fraction of coverage of the adsorbed oxygen species at the interface between the noble metal electrode and the stabilized zirconia solid electrolyte. The double layer capacitance is also potential dependent. When the double layer capacitance was measured as a function of the overpotential, then a maximum was observed at the equilibrium potential as shown in fig. 13. At anodic overpotentials it was difficult to determine the double layer capacitance accurately due to the low value of the electrode impedance and the large inductance of the measuring devices.

The observed potential dependence of the apparent double layer capacitance is in the opposite direction compared with the results obtained by Chebotin et al. [30]. In that study the electric double layer capacitance was determined by impedance measurements with a liquid metal electrode in an oxygen free atmosphere. A minimum was observed in the capacitance versus potential curve. The value of the double layer capacitance was about a factor 10 smaller than observed in our study. In our opinion this observed difference originates from the adsorption of oxygen species between the metal electrode and solid electrolyte surface. This adsorbed oxygen was certainly present in our study but not in their study due to the low oxygen partial pressure (10^{-10}-10^{-18} atm).

The double layer capacitance is assumed to be in parallel to the Faradaic impedance of the electrode. This Faradaic impedance contains information about the charge transfer process, the adsorption of intermediates and mass transport limitations, if present.

The major contribution to the Faradaic impedance of the electrode results from the charge transfer resistance, R_{ct}, which is temperature dependent with an activation energy of (89 ± 2) kJ mol^{-1} and is oxygen partial pressure dependent according to: $R_{ct} \propto Po_2^{-(0.53\pm0.01)}$.

The potential dependence of the electrode resistance (R_{el}), shown in fig. 12, correlates with the values of the apparent anodic and cathodic charge transfer coefficients, obtained from the Tafel plot of fig. 4. The electrode resistanc, R_{el}, is mainly determined by the charge transfer resistance, R_{ct}. Hence it was expected to find the same activation energy (112 ± 2 kJ mol^{-1}) and oxygen partial pressure dependence ($m=0.60\pm0.02$) of R_{ct} as observed for the equilibrium exchange current density, because the following relation exists for a pure charge transfer reaction:

$$R_{el}(\eta=0) = \frac{RT}{(\alpha_c+\alpha_a)FI_o} \qquad (5)$$

Some deviation (up to 20 kJ mol^{-1}) occurs due to the temperature and oxygen partial pressure dependence of the apparent charge transfer coefficients, and due to the contribution of the additional elements R2 and CPE2 in the equivalent circuit which determine also the rate of the oxygen exchange reaction.

All other equivalent circuit elements (R2 and CPE2) which are present in series with the charge transfer resistance, R_{ct}, in fig. 10 may result from the adsorption of intermediate species in the reaction mechanism, from mass transport limitations or other processes which determine the rate of the reaction.

At the Au,O_2(g)/yttria stabilized zirconia interface capacitive and inductive loops have been observed at low frequencies in the impedance diagram during both cathodic and anodic polarisation, and the results are shown in fig. 11 and tabulated in Table I. *Especially inductive loops in the impedance diagram can be related to the transfer of electrons in a stepwise fashion to adsorbed intermediates [1].* Such a stepwise electron transfer takes place in the reaction mechanisms of the eqs (3a-c) and (4a-d). The charge transfer mechanism of the eqs (4a-d) proved to be too complicated to be solved analytically in the way as described in Part I [1]. Due to non-linear equations the fraction of coverage of the adsorbed oxygen species could only be obtained numerically. Linearisation of the equations which describe the electron transfer at the electrode yield formulae which describe the faradaic impedance of the electrode reaction. Due to the fast increase in the number of intermediates and number of kinetic constants of which the values are difficult to estimate, no further analysis was attempted with this complicated reaction mechanism.

Hence the observed inductive effects at low frequencies in the impedance measurements of the Au,O_2(g)/yttria stabilized zirconia interface are discussed in view of the simpler reaction model as shown in the eqs (3a-c). The set of equations belonging to this reaction model could be solved analytically. The mathematical analysis was presented in Part I [1]. It should be noted, however, that the predicted oxygen partial pressure dependence of the equilibrium exchange current density (I_o) in this model ($m=0.29$) is in contradiction with the measurements ($m=(0.60\pm0.02)$), and large deviations are observed from the measured current-overpotential curve

during anodic polarisation. The discrepancy in the oxygen partial pressure dependence of I_o is due to the fact that in the reaction model given in the eqs (3a-c) mass transport limitation have been ignored. A model where mass transport has been taken into account has been discussed in section 6.2.2 of Part I, and can explain the large oxygen partial pressure dependence of I_o.

In the reaction mechanism of the eqs (3a-c), electrons are transfered in a stepwise fashion to two adsorbed intermediates, i.e. O_{ad} and O^-_{ad}. Using the parameter set given in table 1 of Part I, the fraction of coverage of the O_{ad} and O^-_{ad} species at steady state can be calculated from the eqs (5) and (7) in Part I [1]. The adsorption/-desorption kinetics were chosen to be fast in comparison to the charge-transfer process given by eqs (3b) and (3c). This results in a fraction of coverage of the O_{ad} species which is essentially independent of the polarisation over a broad potential range, as shown in fig. 20. The potential dependence of the fraction of coverage of the O^-_{ad} species is more complicated and is related to inductive and capacitive loops in the impedance diagrams.

In order to find an inductive loop in the impedance diagram at cathodic overpotentials, it was found that the cathodic rate constant of step (3b) (k_{r1}) has to increase faster than the cathodic rate constant of step (3c) (k_{r3}) when the cathodic overpotential is increased (more negative). Under such conditions, an increase of the absolute value of the cathodic overpotential results in an increase of the fraction of coverage of the O^-_{ad} species. Such an increase of the fraction of coverage of one of the intermediates can manifest itself as an inductive loop in the impedance diagram at cathodic overpotentials. In order to find the necessary potential dependence of the rate constants, mentioned above, the symmetry coefficients should be different (see eq. (4) in Part I [1]). In the reaction mechanism of eqs (3a-c), the symmetry coefficient of step (b) should be larger than the symmetry coefficient of step (c), in order to simulate the inductive loop at cathodic overpotentials.

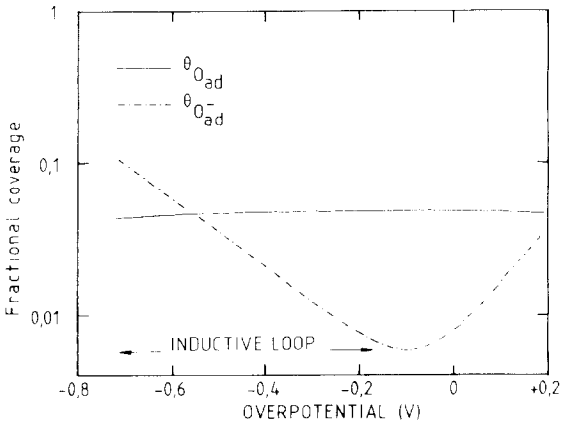

Fig.20 Fraction of coverage of the adsorbed oxygen species O_{ad} and O^-_{ad} as function of the overpotential at 763°C and PO_2=1 atm. Computer simulation based on the reaction mechanism of eqs (3a-c).

The final result of the computer simulation of the electrode impedance as a function of the overpotential is shown in fig. 21. If the simulated electrode impedance diagrams are compared with the measured ones (fig. 11) it is obvious that in both figures a change is observed from an inductive loop at cathodic overpotentials towards a capacitive loop at equilibrium and during anodic polarisation. However, the results from the computer simulation are still far from a mathematical exact description of the observed electrode impedance.

A further analysis of the results is complicated by the observed frequency dispersion of the elements in the equivalent circuit, as shown in table 1. The computer simulation predicts always pure capacitive (n=+1) and inductive (n=-1) elements in the equivalent circuit when no mass-transport limitations are taken into account. In the impedance diagrams of this study, constant phase elements have been observed with exponent values of $-0.79 < n < -0.39$ (inductive loop) or $+0.48 < n < +1$ (capacitive loop), as presented in table 1. Those constant phase elements present themselves as depressed semi-circles in the impedance diagram when they are parallel to a resistor. No process has been conceived so far which could explain such a large degree of depression of the inductive loop in the impedance diagram.

A constant phase element with an exponent value of n=+0.5 is equivalent to a Warburg impedance when the diffusion of the electroactive species takes place in a semi infinite medium. A parallel combination of such a Warburg impedance with a resistance results in a quarter circle in the impedance diagram. Braunshtein et al. [31] discussed the physical significancy of such a combination of circuit elements in describing the electrode reaction at the Pt,O_2/yttria stabilized zirconia interface. They explained their results by suggesting that part of the oxygen atoms is directly incorporated at the three phase boundary and the remaining part diffuses along the electrode/electrolyte interface with the charge transfer taking place in this two phase region. A more exact treatment of this mass transport problem and the consequences for the electrode impedance was given by Franceschetti and Ross [32], and presented in Part I [1], showing that at equilibrium a competition between charge transfer and diffusion in the two phase region at the electrode/electrolyte interface results in a pure capacitive loop in the impedance diagram. The depression of the capacitive and inductive loops in the impedance diagram

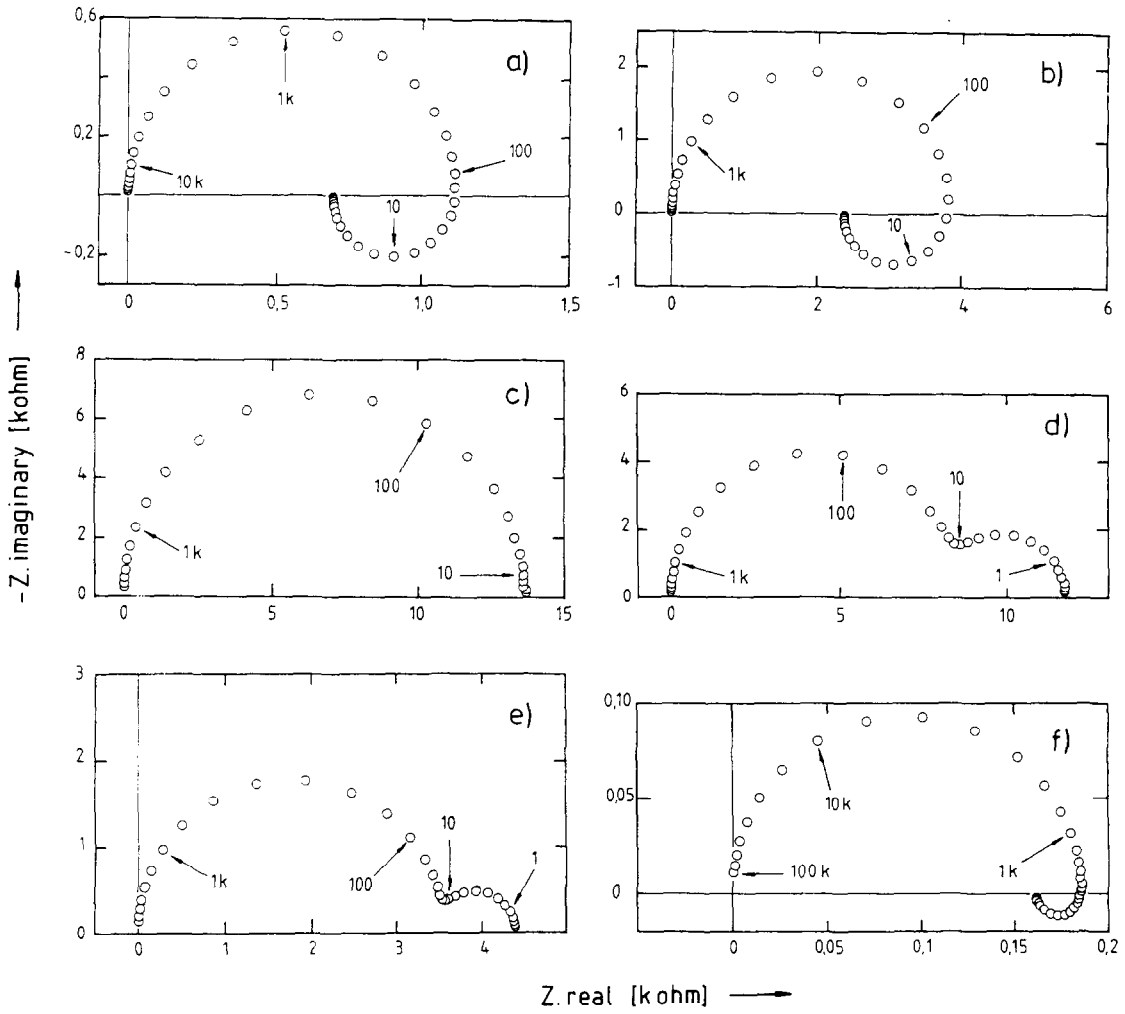

Fig.21 Simulated impedance diagrams (763°C, PO_2=1 atm) based on the reaction mechanism given in the eqs (3a-c) using the paramaters of table 1 in Part I [1]. Calculations performed at the following overpotentials: a) η=-0.6 V, b) η=-0.4 V, c) η=-0.1 V, d) η=0 V, e) η=0.1 V, f) η=0.4 V. Frequencies indicated in Hz.

remains a problem to be solved. In our opinion the discrepancy between the frequency dispersion of the simulated capacitive and inductive elements and the measured ones results from mass transport limitations and possibly inhomogeneous current distributions but no exact treatment has yet been obtained.

5. Conclusions

A combination of steady state polarisation measurements and impedance measurements as a function of the overpotential yields complementary information about the oxygen exchange reaction at the Au,O_2(g)/yttria stabilized zirconia interface.

The steady state polarisation measurements can be explained with a reaction model in which a competition exists between charge transfer and mass transport of molecularly adsorbed oxygen along the Au/yttria stabilized zirconia interface. The experimentally observed apparent cathodic charge transfer coefficient of α_c=0.5 and oxygen partial pressure dependence of the apparent equilibrium exchange current density (m=0.60±0.02) support this conclusion. The apparent anodic charge transfer coefficient ($1.7<\alpha_a<2.8$) deviates however from the model prediction (α_a=1.5).

The impedance measurements as a function of the overpotential provide information about the reaction mechanism and about the potential dependence of the fraction of coverage of the adsorbed oxygen species. The electrode impedance is largely determined by the charge transfer resistance parallel to a double layer capacitance, but at low frequencies deviations are observed. During cathodic polarisation inductive loops appear at low frequencies in the impedance diagram, which are related to a change of the fraction of coverage of adsorbed oxygen species when the electrode potential is modulated. A model analysis shows that inductive effects at cathodic overpotentials appear when the fraction of coverage of one of the adsorbed oxygen species increases with more negative values of the cathodic overpotential.

The interpretation of the impedance measurements as a function of the overpotential is complicated by the frequency dispersion of the observed elements in the equivalent circuit. Instead of finding pure capacitive and inductive elements, constant phase elements were observed with exponent values in the range of $+0.48 < n < +1$ and $-0.79 < n < -0.39$, respectively. The frequency dispersion of those capacitive and inductive elements hinder the development of a reaction model which can simulate the electrode impedance quantitatively.

A further complication is the incompatibility of the equivalent circuit used in the NLLS-fit analysis (fig. 10) with the circuit that follows from the reaction model based on the exchange reaction of eqs (3a-c) (Part I, fig. 3). As diffusion clearly is involved in the electrochemical oxygen exchange reaction the model equivalent circuit developed in Part 1 is obviously too simple. A more complete analysis including this diffusion step would result in a more complex model circuit. It is however conceivable that some circuit elements do not contribute significantly to the total dispersion. This then will lead to a simplified model circuit, possibly with an apparent arrangement of elements as used in the analysis here (see fig. 10).

Acknowledgement

The foundation SGM is thanked for putting their SIMS facility at our disposition. Especially D. Gras and A.P. von Rosenstiel are thanked for their assistance. The investigations were supported by the Netherlands Foundation for Chemical Research (SON) with financial aid from the Netherlands Organisation for Scientific Research (NWO).

References

[1] B.A. van Hassel and A.J. Burggraaf, '*Electrode Polarization at Au, O_2(g)/stabilized zirconia interface. Part I: Theoretical Considerations of Reaction Model*', Solid State Ionics, in press.
[2] B.A. van Hassel, Transport and oxygen transfer properties of ion implanted yttria stabilized zirconia, PhD Thesis, University of Twente, Enschede, The Netherlands (1990).
[3] B.A. van Hassel, B.A. Boukamp and A.J. Burggraaf, submitted for publication.
[4] M. Grasserbauer, H.J. Dudek and M.F. Ebel (eds.), Angewandte oberflächen Analyse mit SIMS, AES, XPS, (Springer Verlag, Berlin, Heidelberg, New York, Toronto 1985).
[5] H. Yanagida, R.J. Brook and F.A. Kröger, J. Electrochem. Soc. **117** (1970) 593.
[6] B.A. Boukamp, Solid State Ionics **20** (1986) 31.
[7] B.A. Boukamp, "Equivalent Circuit", Internal Report CT89/214/128, University of Twente 1989.
[8] P. Légaré, L. Hilaire, M. Sotto and G. Maire, Surface Science **91** (1980) 175.
[9] N.D.S. Canning, D. Outka and R.J. Madix, Surface Science **141** (1984) 240-254
[10] J.J. Pireaux, M. Chtaïb, J.P. Delrue, P.A. Thiry, M. Liehr and R. Caudano, Surface Science **141** (1984) 211.
[11] J.J. Pireaux, M. Liehr, P.A. Thiry, J.P. Delrue and R. Caudano, Surface Science **141** (1984) 221.
[12] M.A. Chesters and G.A. Somorjai, Surface Science **52** (1975) 21.
[13] D.D. Eley and P.B. Moore, Surface Science **76** (1978) L599.
[14] M. Haruta, H. Kageyama, N. Kamijo, T. Kobayashi and F. Delannay in "Successfull Design of Catalysts, T. Inui (Editor), Elsevier Science Publishers B.V., Amsterdam (1988) 33-42.
[15] M. Haruta, N. Yamada, T. Kobayashi and S. Iijima, Journal of Catalysis **115** (1989) 301.
[16] Y. Meas, J. Fouletier, D. Passelaigue et M. Kleitz, Journal de Chimie Physique **75** (1978) 826.
[17] T. Smith, J. Electrochem. Soc. **11** (1964) 1020.
[18] T. Smith, J. Electrochem. Soc. **11** (1964) 1027.
[19] E.Kh. Kurumchin, M.V. Perfil'ev, S.V. Karapachev and V.S. Muzykantov, Kinetika i Kataliz, **17**, (1976) 1519.
[20] D.S. Tannhauser, J.A. Kilner and B.C.H. Steele, Nucl. Inst. and Methods in Physical Research **218** (1983) 504.
[21] B.C.H. Steele, J.A. Kilner, P.F. Dennis, A.E. McHale, M. van Hemert and A.J. Burggraaf, Solid State Ionics **18&19** (1986) 1038.

[22] M. Che and A.J. Tench, Advances in Catalysis, **Vol. 31**, 77.
[23] M. Che and A.J. Tench, Advances in Catalysis, **Vol. 32**, 1.
[24] W. Göpel, Progress in Surface Science, Vol. 20(1), (1985) pp. 9-103.
[25] J. Mizusaki, K. Amano, S. Yamauchi and K. Fueki, Solid State Ionics **22** (1987) 313.
[26] J. Mizusaki, K. Amano, S. Yamauchi and K. Fueki, Solid State Ionics **22** (1987) 323.
[27] B.C. Nguyen, L.M. Rincon-Rubio and D.M. Mason, J. Electrochem. Soc. **133** (1986) 1860.
[28] E.J.L. Schouler and M. Kleitz, J. Electrochem. Soc. **134** (1970) 1045.
[29] S.P.S. Badwal and F.T. Ciacchi, Solid State Ionics **18&19** (1986) 1054.
[30] V.N. Chebotin, I.D. Remez, L.M. Solovieva and S.V. Karpachev, Electrochimica Acta, **29** (1984) 1381.
[31] D. Braunshtein, D.S. Tannhauser and I. Riess, J. Electrochem. Soc. **128** (1981) 82.
[32] D.R. Franceschetti and A.P. Ross, Appl. Phys. **A49** (1989) 111.